Journal of Physics and Chemistry of Solids 104 (2017) 192–197

Contents lists available at ScienceDirect

Journal of Physics and Chemistry of Solids

journal homepage: www.elsevier.com/locate/jpcs

Simple model dielectric functions for insulators

Maarten Vos[a,*], Pedro L. Grande[b]

[a] Electronic Materials Engineering Department, Research School of Physics and Engineering, The Australian National University, Canberra 2601, Australia
[b] Ion Implantation Laboratory, Instituto de Física, Universidade Federal do Rio Grande do Sul, Av. Bento Goncalves, 9500, CP 15051, CEP 91501-970, Porto Alegre, RS, Brazil

ARTICLE INFO

Keywords:
Dielectric function
Inelastic x-ray scattering
Compton scattering
Water
Diamond

ABSTRACT

The Drude dielectric function is a simple way of describing the dielectric function of free electron materials, which have an uniform electron density, in a classical way. The Mermin dielectric function describes a free electron gas, but is based on quantum physics. More complex metals have varying electron densities and are often described by a sum of Drude dielectric functions, the weight of each function being taken proportional to the volume with the corresponding density. Here we describe a slight variation on the Drude dielectric functions that describes insulators in a semi-classical way and a form of the Levine-Louie dielectric function including a relaxation time that does the same within the framework of quantum physics. In the optical limit the semi-classical description of an insulator and the quantum physics description coincide, in the same way as the Drude and Mermin dielectric function coincide in the optical limit for metals. There is a simple relation between the coefficients used in the classical and quantum approaches, a relation that ensures that the obtained dielectric function corresponds to the right static refractive index.

For water we give a comparison of the model dielectric function at non-zero momentum with inelastic X-ray measurements, both at relative small momenta and in the Compton limit. The Levine-Louie dielectric function including a relaxation time describes the spectra at small momentum quite well, but in the Compton limit there are significant deviations.

1. Introduction

Dielectric functions are pervasive in condensed matter physics. However, the full energy (ω) and momentum ($\boldsymbol{q}$) dependence of the dielectric function ($\epsilon(\omega, q) = \epsilon_1(\omega, q) + i\epsilon_2(\omega, q)$ with ϵ_1, ϵ_2 real) show intricate structures (see e.g. [1]) and is usually not fully known and thus widespread use is made of model dielectric functions. Knowledge of the dielectric function is also essential in medical physics to understand the penetration of charged particles in an organisms and the distribution of the associated 'damage'. The use of the dielectric function in this context has been reviewed recently [2]. Here we want to highlight some elementary properties of dielectric functions and present an alternative model dielectric function that can be of use for insulators.

2. Model dielectric functions

A frequently used model for metals is the Drude one based on the free-electron model which assumes that the target electrons have a homogeneous electron density. This Drude function (ϵ_D) is based on a classical approach and the energy loss function (ELF) $\mathrm{Im}\left[\frac{-1}{\epsilon_D(\omega, q)}\right]$ is given by:

$$\mathrm{Im}\left[\frac{-1}{\epsilon_D(\omega, q)}\right] = \frac{\omega\Gamma(q)\omega_i(0)^2}{(\omega^2 - \omega_i(q)^2)^2 + \omega^2\Gamma(q)^2} \quad (1)$$

and the corresponding real part:

$$\mathrm{Re}\left[\frac{1}{\epsilon_D(\omega, q)}\right] = 1 + \frac{(\omega^2 - \omega_i(q)^2)\omega_i(0)^2}{(\omega^2 - \omega_i(q)^2)^2 + \omega^2\Gamma(q)^2}. \quad (2)$$

Here the plasma frequency ω_i is determined by the electron density N ($\omega_i = \sqrt{4\pi N}$, we use atomic units throughout, unless otherwise stated) and Γ is a damping constant. Both ω_i and Γ can depend on q, but for the Drude model we assume in the following that Γ does not depend on q.

For cases where the electron density is in-homogeneous one may consider the target as a sum of volumes with different electron densities. A volume fraction C_i has an electron density such that the plasmon energy is ω_i. The sum of all volume fraction should obviously add up to one: $\sum_i C_i = 1$. The dielectric function is then given by a weighted sum of their Drude functions. This approach has been quite

* Corresponding author.
E-mail address: maarten.vos@anu.edu.au (M. Vos).

http://dx.doi.org/10.1016/j.jpcs.2016.12.015
Received 1 December 2016; Accepted 15 December 2016
Available online 23 December 2016
0022-3697/

useful for the determination of the ion stopping [3]. as well as the electron mean free path [4,5]. The corresponding ELF is then:

$$\mathrm{Im}\left[\frac{-1}{\epsilon(\omega, q)}\right] = \sum_i C_i \frac{\omega\Gamma_i\omega_i(0)^2}{(\omega^2 - \omega_i(q)^2)^2 + \omega^2\Gamma_i^2} \tag{3}$$

and for the real part:

$$\mathrm{Re}\left[\frac{1}{\epsilon(\omega, q)}\right] = \sum_i C_i\left[1 + \frac{(\omega^2 - \omega_i(q)^2)\omega_i(0)^2}{(\omega^2 - \omega_i(q)^2)^2 + \omega^2\Gamma_i^2}\right] \tag{4}$$

Note that Eqs. (3) and (4) only satisfy the Kramers-Kronig relations when $\sum C_i = 1$.

Lindhard developed a quantum formulation of the dielectric function ($\epsilon_L(\omega, \boldsymbol{q})$) for a free-electron material and vanishing relaxation time [6]. Mermin added later the effect of a finite relaxation time (i.e. damping) [7]:

$$\epsilon_M(\omega, \boldsymbol{q}) = 1 + \frac{(1 + i\Gamma/\omega)(\epsilon_L(\omega + i\Gamma, \boldsymbol{q}) - 1)}{1 + i\Gamma/\omega[\epsilon_L(\omega + i\Gamma, \boldsymbol{q}) - 1]/[\epsilon_L(0, \boldsymbol{q}) - 1]} \tag{5}$$

and both Lindhard and Mermin dielectric functions are widely used. For q=0 the Mermin dielectric function (ϵ_M) and the semi-classical Drude one coincide.

Levine and Louie derived a dielectric function for insulators (ϵ_{LL}) by transforming the energy scale of the imaginary part of the Lindhard dielectric function according to $\omega'^2 = \omega^2 + U^2$ (with U a parameter that relates to, but is not equal to the band gap), and calculating the real part using Kramers-Kronig relations [8]. Here we first extend the Levine-Louie approach by adding a relaxation time in the same way as Mermin did to the Lindhard dielectric function by replacing ϵ_L in Eq. (5) by ϵ_{LL} and refer to this as the ϵ_{MLL} (Mermin-Levine-Louie) dielectric function. Examples for ϵ_{MLL} for a single component with $\omega_1^M = 10$ eV, $\Gamma_1 = 2$ eV and U values as indicated are given in Fig. 1. With increasing U values the position of maximum intensity of the ELF, moves to larger ω values, its area decreases in such a way that the value of the Bethe sum rule:

$$\frac{1}{2\pi^2}\int_0^\infty \omega'\mathrm{Im}\left[\frac{-1}{\epsilon(\omega', 0)}\right]d\omega' = N \tag{6}$$

remains the same. Here N is the target electron density which, for $\omega_1 = 10$ eV, corresponds to 0.01075 electrons/(a.u)^3.

In order to consider the shape of such a single component MLL ELF more carefully, we take the case of U=16 eV of Fig. 1 as an example. Its shape is still in good approximation a Lorentzian with the same width as the loss function for U=0 (upper panel Fig. 2). Here we compare it with the result for Eq. (1) using $\omega^D = \sqrt{\omega^{dens} + U^2}$ and $\Gamma_1 = 2$. (In the following we use ω^D, ω^M and ω^{MLL} for the ω parameter in the Drude, Mermin and MLL model. ω^{dens} is the plasma frequency that corresponds to the electron density of the target ($\omega^{dens} = \sqrt{4\pi N}$). Note that $\omega^{MLL} = \omega^{dens}$ by definition. The position and width of the Drude and MLL ELFs are then the same, but the area of the Drude one is much larger. As a consequence its Bethe sum is much larger i.e. it corresponds to a target with a much larger electron density.

One can rescale the Drude ELF by using Eq. (3) with $C^D = (\omega_1^{dens}/\omega_1^D)^2 = 0.278$ and then at q=0 both ELFs coincide. The question is then what happens with fraction of the volume $1 - C = 0.722$. It turns out that one obtains internally consistent results if it is treated as 'empty' or 'vacuum' i.e. this fraction contributes to the dielectric function with $\epsilon_1 = 1$ and $\epsilon_2 = 0$ (or equivalently $Re\,[1/\epsilon(\omega, q)] = 1$ and $\mathrm{Im}\,[-1/\epsilon(\omega, q)] = 0$) and here we refer to this approach as 'Drude+vacuum'. The real part of Eq. (3) reads:

$$\mathrm{Re}\left[\frac{1}{\epsilon(\omega, q)}\right] = \sum_i C_i^D\left[1 + \frac{(\omega^2 - \omega_i^D(q)^2)\omega_i^D(0)^2}{(\omega^2 - \omega_i^D(q)^2)^2 + \omega^2\Gamma_i^2}\right] + 1 - \sum_i C_i^D$$
$$= 1 + \sum_i C_i^D\left[\frac{(\omega^2 - \omega_i^D(q)^2)\omega_i^D(0)^2}{(\omega^2 - \omega_i^D(q)^2)^2 + \omega^2\Gamma_i^2}\right] \tag{7}$$

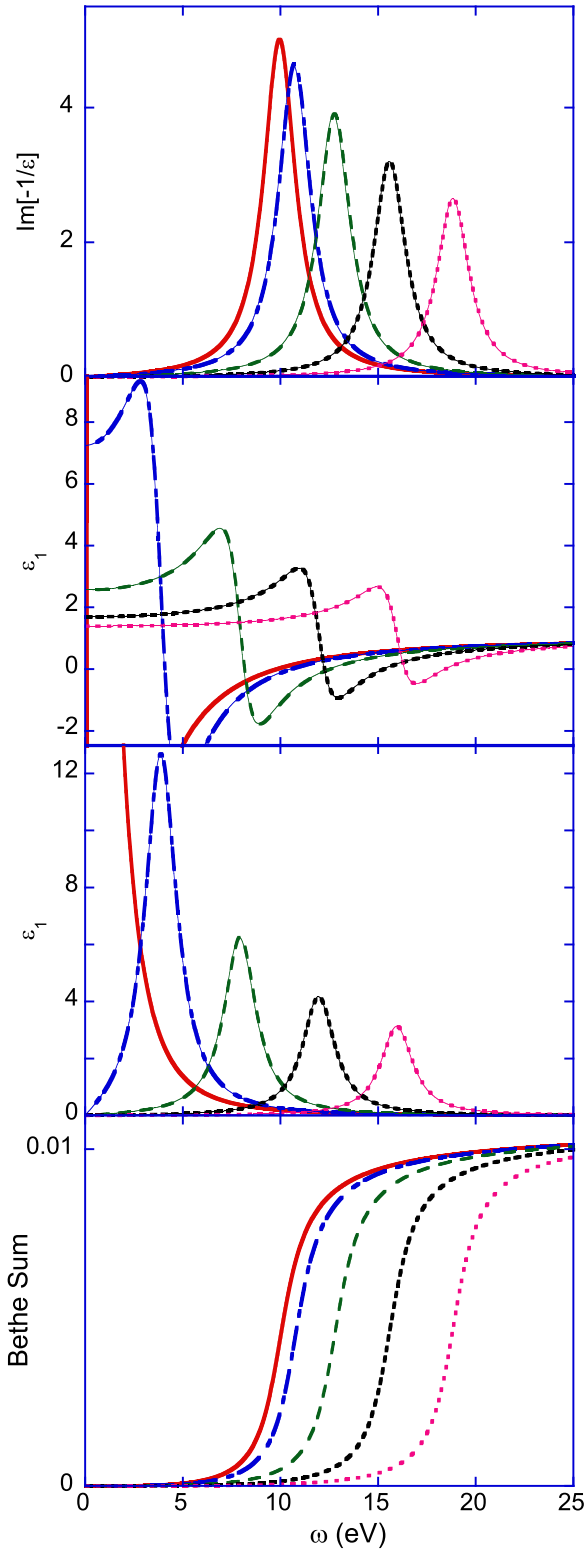

Fig. 1. The top panel shows (thick lines) the ELF for a single oscillator with ω = 10 eV and Γ = 2 eV for the 'Mermin-Levine-Louie' model for U values (in eV) as indicated. The central panels show the real and imaginary part of the corresponding dielectric function. The thin lines in these plots are the same quantities using a very simple Drude+vacuum model as explained in the text. The bottom panel shows the development of the Bethe sum integral (Eq. (6)) as a function of upper limit of the integration.

while the imaginary part remains unchanged. Note that Eqs. (3) and (7) satisfy Kramers-Kronig relations, even if $\sum C_i^D < 1$. Using this interpretation with volume $1 - \sum_i C_i^D$ treated as vacuum

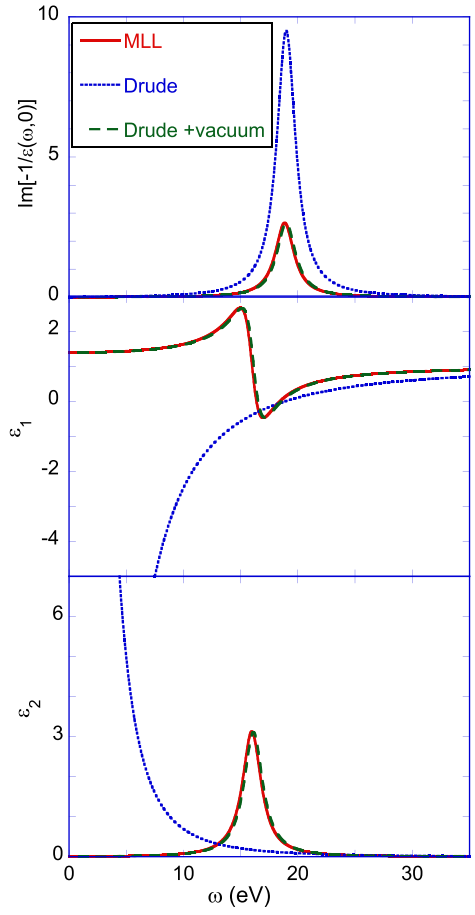

Fig. 2. The ELF, ϵ_1 and ϵ_2 for a Mermin-Levine-Louie oscillator with $\omega_1 = 10$, $\Gamma_i = 2$ and U=16, an Drude oscillator with $\omega = 18.86$ and $\Gamma = 2$ (dotted line) and the same oscillator multiplied by 0.278 plus a vacuum with volume fraction (1-0.278)(long dash).

$1/\epsilon_1 \rightarrow 1 - \sum_i C_i^{\mathrm{D}}$ when $\omega \rightarrow 0$. There is thus a simple relation between the 'empty fraction' and the static refractive index n of a material: $n^2 = \epsilon_1(0, 0) = 1/(1 - \sum C_i^{\mathrm{D}})$, as will be discussed in more detail in Section 3.

Now let us compare the shape of the real and imaginary part of $\epsilon(\omega, q)$ for both the Drude, and MLL model. At q=0 ϵ_1 and ϵ_2, as calculated by both models, are identical (central and lower panel of Fig. 2). Here we claim that this approach of a Drude oscillator+vacuum is the semi-classical equivalent to the MLL ELF, in the same way as the Drude ELF is the semi-classical equivalent to the Mermin ELF. In the limit of q=0 they are indistinguishable, but will differ for $q \neq 0$.

Instead of the Drude ELF one can also consider the Mermin ELF with the same parameters ($\omega_1^M = \sqrt{\omega_1^{dens^2} + U^2}$, and $C_1^{\mathrm{M}} = (\omega_1^{\mathrm{dens}}/\omega_1^{\mathrm{M}})^2$) and if one treat again $1 - C_1^{\mathrm{M}}$ as vacuum one obtains at q=0 again the same description for ϵ_1, ϵ_2 and thus Im $[-1/\epsilon]$.

The behavior away from q=0 is demonstrated in Fig. 3, assuming for the Drude case a free-electron type dispersion: $\omega_1^{\mathrm{D}}(q) = \omega_1^{\mathrm{D}}(0) + q^2/2$ (in the other cases dispersion is 'build in'). Now all 3 dielectric functions start to differ, especially for $q > 0.5$ a.u. The Drude ELF remains sharply peaked whereas the Mermin ELF becomes very broad. For the MLL ELF the broadening is less severe, in particular the MLL ELF has a strongly reduced intensity (but is not strictly zero) for losses considerable less than U.

At even larger q values one reaches the 'Bethe ridge' where the interaction between probe and target electrons can be described as binary collisions [9]. In this Compton regime there is a simple relation between the momentum of the scattering electron $\boldsymbol{p}$ and the energy loss ω:

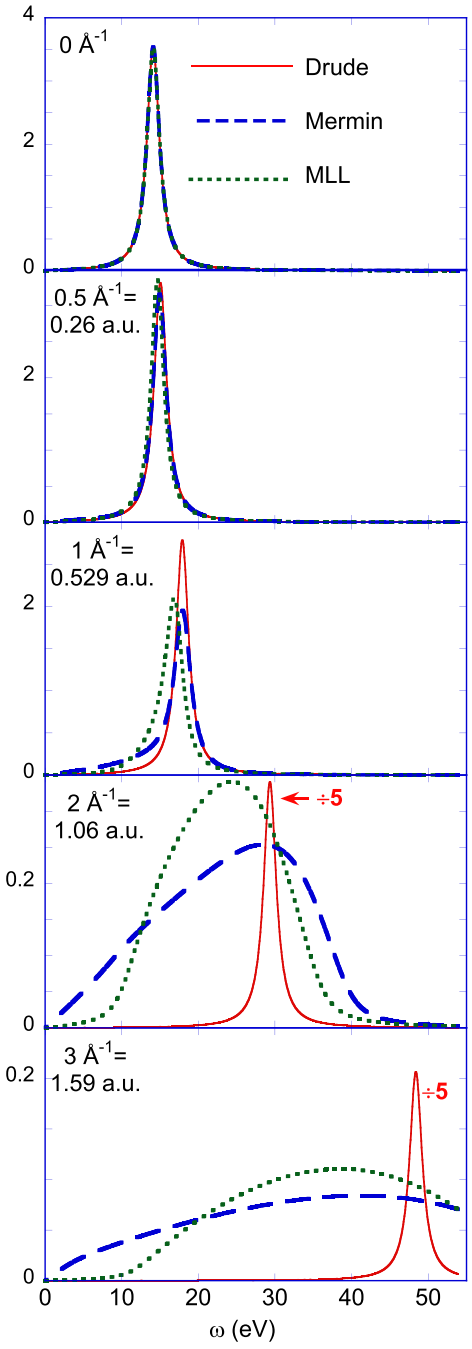

Fig. 3. The development of the ELF as a function of momentum transfer for the Drude loss function (ω = 14.14 eV, C=0.5, Γ = 2 eV and α = 1), Mermin dielectric function (ω = 14.14 eV, C=0.5, Γ = 2) and Mermin-Levine-Louie loss function (ω = 10 eV, U=10 eV, C=1, Γ = 2 eV).

$$\omega = \frac{q^2}{2\,m} + \frac{\boldsymbol{q}\cdot\boldsymbol{p}}{m} \tag{8}$$

with m the electron mass (equal to 1 in atomic units). The various dielectric functions at high momentum transfer are displayed in Fig. 4 for q=20 a.u. in terms of both the energy loss and the component of $\boldsymbol{p}$ along $\boldsymbol{q}$. The Drude ELF remains very narrow, in contrast to Compton peaks observed in experiments. The MLL ELF has a width that corresponds to the Fermi sphere of a free-electron gas with a plasmon energy of $\omega^{\mathrm{MLL}} = 10$ eV. The Mermin-derived Compton profile has a width corresponding to a free-electron gas with a plasmon energy of ω^{M} (14.14 eV). For wide-gap insulators it should thus be possible to distinguish experimentally which

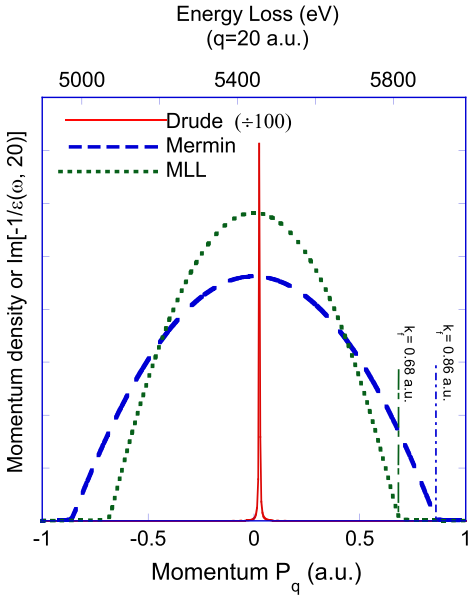

Fig. 4. The ELF at q=20 a.u. for the same dielectric functions plotted in Fig. 3, Now the result can be interpreted as a Compton profile, i.e. intensity is proportional to the density of target electrons with a certain momentum p along the momentum transfer direction. In the Drude case the width is still 2 eV, In the Mermin case the width corresponds to that of a free-electron gas with plasmon energy 14.14 eV and hence k_f=0.86 a.u., in the Mermin-Levine-Louie case the width corresponds to a free electron gas with plasmon energy 10 eV (k_f=0.68 a.u.).

of these two approaches describe the data best.

3. Examples: diamond and water

Let us first consider the case of diamond as an example. The book of Raether gives a table comparing observed plasmon energies with the calculated value for a range of materials [10]. Diamond stands out somewhat as its observed plasmon energy (34 eV) is significant larger than the calculated plasmon energy (ω^{dens} = 31 eV). The latter value is ω^{MLL}, the observed peak position would correspond to ω^{D}. Within the MLL model the peak position would be explained if $U = \sqrt{\omega^{\mathrm{D}^2} - \omega^{\mathrm{dens}^2}} \approx 14$ eV, a value considerable larger than the band gap of diamond. Alternatively one can describe it with a Drude model model plus empty fraction. Now we get for the coefficient $C^{\mathrm{D}} = (\omega^{\mathrm{dens}}/\omega^{\mathrm{D}})^2 = 0.83$, which corresponds to an empty fraction of 0.17. The static refractive index can then be calculated using $n^2 = 1/(1 - \sum C_i)$ which gives an n value of 2.4, in surprisingly good agreement of the established value of 2.4. (We use the experimentally obtained refractive index at ω = 1 eV for the 'static refractive index' to avoid the phonon contribution throughout this paper). These numbers are reproduced in Table 1.

Table 1
Various quantities for diamond and water, as discussed in the main text. ω^{dens} is the calculated plasmon energy based on the (average) valence electron density, $\omega^{\mathrm{obs.}}$ is the position of the maximum of the ELF. For water we give in brackets the plasmon energy as inferred from the average energy loss of the ELF. Within the MLL model U inf. is the estimate of this parameter based on $U = \sqrt{\omega^{\mathrm{obs}^2} - \omega^{\mathrm{dens}^2}}$. Within the Drude or Mermin model the inferred 'empty fraction' (E. F.) is given by $1 - (\omega^{\mathrm{dens}}/\omega^{\mathrm{obs}})^2$ and the refractive index n is then obtained from $n^2 = 1/(\mathrm{E.\ F.})$. The last column is the measured refractive index.

Material	ω^{dens}	ω^{obs}	U inf.	empty frac.	n inf.	n obs.
Diamond	31.1	34	13.7	0.16	2.5	2.4
water	19.2	23.5 (30.4)	13.6 (23.5)	0.33 (0.6)	1.74 (1.29)	1.32

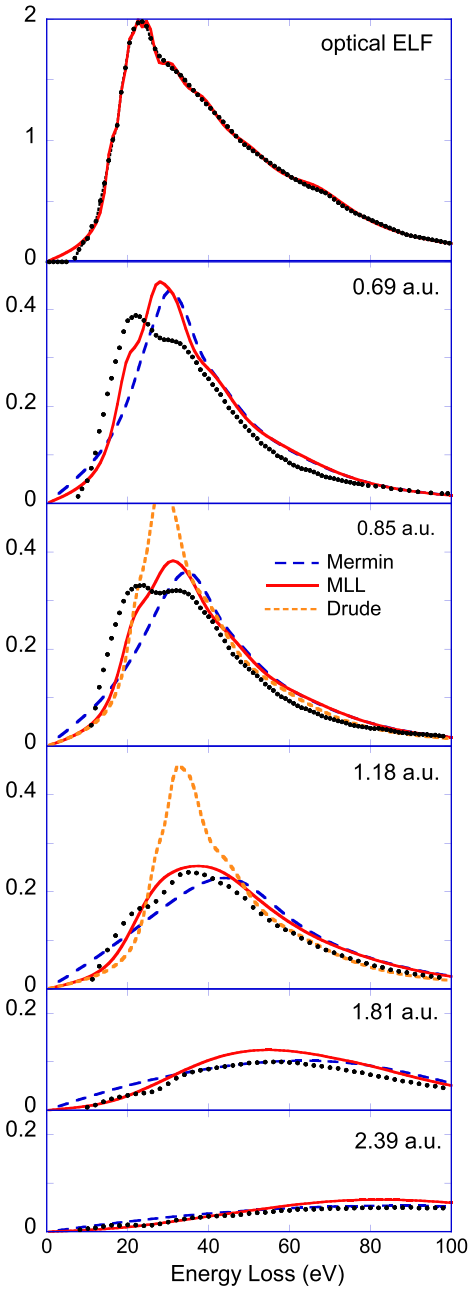

Fig. 5. A comparison of the measured values of Im [− 1/ϵ(ω, q)] (dots) at the q values as indicated with the corresponding curves for the Mermin, Mermin-Levine-Louie as well as the Drude model ELF.

For water one can also try to make such a comparison but the ELF is rather asymmetric. One can either equate the experimentally observed plasmon energy with the position of the maximum of the ELF, or with its mean value. These choices result in rather different U values and hence calculated refractive indexes. The derived values from both choices of observed plasmon energy are given in Table 1 as well. The experimental value of the refractive index is in between the values derived for both choices of plasmon energies.

For the case of water there exist inelastic X-Ray Scattering Spectroscopy (IXSS) measurements of the dielectric function near the optical limit [11,12] and away from q=0 [13], as well as Compton measurements at very large q values, see e.g. ref. [14]. Due to the relevance of the dielectric function of water in medical physics detailed somewhat semi-empirical parametrisations of this quantity exist [15–17]. Here we want to review how well in particular the MLL model

Table 2
The parameters of the fit of the ELF in the optical limit as measured by Hayashi et al. [11] using the Mermin or Drude model (left half) or the MLL model (right half). The parameters in the right and left half of the table are linked via Eqs. (9) and (10).

Drude, Mermin			MLL			
C_i	$\omega_i^{D,M}$ (eV)	Γ_i (eV)	C_i^{MLL}	ω_i^{MLL} (eV)	Γ_i (eV)	U_i (eV)
0.060	17.7	5.9	0.44	6.57	5.9	16.4
0.090	22.4	6.3	0.19	15.2	6.3	16.4
0.096	26.4	8.5	0.16	20.6	8.5	16.4
0.10	35.2	17.5	0.13	31.1	17.5	16.4
0.064	52.5	38.2	0.074	49.6	38.2	16.4
$\sum C_i = 0.41$			$\sum C_i = 1$			

dielectric functions using a set of oscillators describe these data.

The comparison with IXSS measurements are shown in Fig. 5. We used a fit of only 5 components, as this suffices to reproduce the main features. The parameters used are reproduced in Table 2. The fit was done first for a sum of Drude oscillators. The sum of the obtained coefficients C_i is only 0.41 which ensures that the right refractive index is obtained (n=1.3). The same ELF is obtained if we calculate the Mermin ELF with these parameters. As the experiment was put on an absolute scale using a sum rule, a good fit of the experiment implies the correct Bethe sum value.

The MLL calculation is much more time consuming. It is thus most convenient to use the results of the fitting parameters from the Drude fit. The energy ω_i^{dens} is then retrieved by:

$$\omega_i^{dens} = \sqrt{\omega_i^{D^2} - U^2}. \tag{9}$$

The coefficients C_i^{MLL} are obtained from C_i^{D} via

$$C_i^{MLL} = \left(\frac{\omega_i^{D}}{\omega_i^{dens}}\right)^2 C_i^{D} \tag{10}$$

Now the shape of the optical ELF will not change. Note that only for U value used of 16.4 eV the data can be fitted with $\sum_i C_i^{MLL} = 1$ This U value is about twice as big as the value usually quoted for the band gap of water (7–8 eV), stressing the fact that the U parameter can not be directly compared to the band gap.

Away from q=0 the results for the 3 approaches differ significantly as is illustrated in Fig. 5. For the Drude model the shape of the peak does not change, but it moves gradually to larger energy losses. The Mermin model displays the largest broadening, the broadening for the MLL model is somewhat less. The MLL model seems to agree best with the experiment.

Abril et al. [18] compared these measurement with a dielectric function based on the Mermin dielectric function as well. Their results are consistent with ours. They multiplied the Mermin loss function with a step function, zeroing the intensity in the band gap region (0–7 eV energy loss). This improves of course the agreement between experiment and calculation, as far as the loss function is concerned. This zeroing will affect, of course, also the real part of ϵ as they are linked by Kramers-Kronig and the consequences for the expected dispersion is not easily judged, as after zeroing the ELF in the gap the corresponding dielectric function is not quite a Mermin dielectric function. The intensity of the MLL ELF in the band gap region is less than that of the 'pure' Mermin loss function.

Finally we compare the result of the ELF of water in the Compton limit. In the experimental Compton profile of water there are also contributions of the O 1s electrons, which are not considered in the dielectric function. For the O 1s contribution we used the calculated Compton profile from Biggs et al. [19], and the ratio of the area of the O 1s to valence band contribution was set to 1:4, as there are 2 O 1s electrons and 8 valence electrons for each water molecule. The resulting profile is compared with the experimental result of Manninen et al. [14] in Fig. 6. Surprisingly the Mermin Compton profile agrees better with the experiment than the MLL profile and the MLL profile is somewhat too narrow.

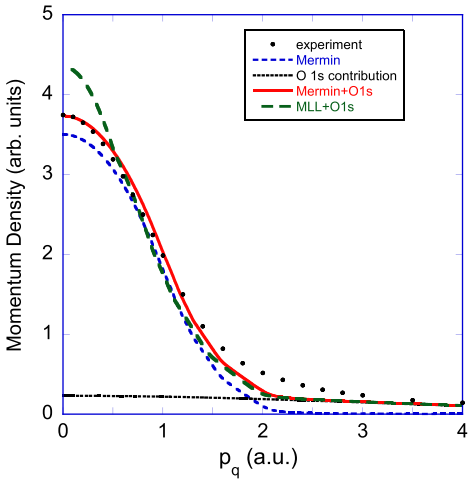

Fig. 6. A comparison of the Compton profile of water, as measured by Manninen et al. [14] with calculated ones. The O 1s contribution (dotted line taken from calculations) is summed with the valence band contribution as modeled by the Mermin and MLL dielectric functions.

A possible cause for the small MLL Compton width could be due to dependence of the intensity of the oscillators on ω. At large ω the ELF decreases as ω^{-3} whereas theory predicts $\omega^{-4.5}$ [2]. Within the Drude model this problem can be diminished by replacing Drude-type oscillators with derivative Drude oscillators, which decrease as ω^{-5}. Fitting the optical ELF with derivative Drude functions would require more oscillators at large energy losses (as the intensity of their tail is less), which would correspond to larger electron densities, and thus cause an increase in the Compton profile width. Incorporating such changes in the Mermin and MLL ELFs is not trivial and was not attempted.

4. Summary and discussion

There are three ways for describing the loss function of an insulator in the optical limit. One can use the (the sum of one or more) MLL loss functions and then one has to choose the coefficients C_i such that they sum up to unity. The gap-like parameter U can be tuned so the correct Bethe sum value and the right static refractive index is obtained. Alternatively one can use the Drude or Mermin loss function and choose the C_i component in such a way that it is less than 1. The missing volume is then treated as having the dielectric function of vacuum. Scaling the C_i coefficient such that the missing fraction changes will again affect both the Bethe sum rule and the static refractive index. Away from q=0 all models give different results. For the case of water the MLL dielectric function seems to reproduce the dispersion at small momentum best. Neither the Mermin or the MLL approach describe the Compton profile perfectly, whereas the Drude approach fails completely.

The origin of the 'empty space' in the crystal is due to areas with electron densities so low that the associated plasmon frequency is less than the band gap. This low-density part contribute to the loss spectrum far away from the plasma frequency corresponding to its density. Hence the area of its loss feature is much reduced, else Bethe sum rule would not be met. These calculations seem to indicate that the net effect is that the material can be modeled as part of its volume is void of electrons. In a way an insulator is not only a material that is void of electrons in a certain energy range (the gap) but for the purpose described here, it may also be seen void of electrons in a certain fraction of its unit cell.

While model dielectric functions are necessarily an oversimplification of the real one, and never will describe the actual one 100% accurately, incorporating as much physics in a model dielectric function should ensure that this function approaches the real one as much as possible and can be used to enhance our understanding of many phenomena. A complete description of the dielectric function can probably only be obtained by large-scale ab-initio calculations based on many-body theory, as has become within reach in recent years [20].

Acknowledgements

This work was made possible by a grant of the Australian Research Council. P.L.G. acknowledges funding from the Braziian agencies CNPq, INES and FAPERGS. The authors thank Nestor Arista for the suggestion of using MLL dielectric function.

References

[1] A. Alkauskas, S. Schneider, C. Hébert, S. Sagmeister, C. Draxl, Dynamic structure factors of Cu, Ag, and Au: comparative study from first principles, Phys. Rev. B 88 (2013) 195124. http://dx.doi.org/10.1103/physrevb.88.195124.

[2] H. Nikjoo, D. Emfietzoglou, T. Liamsuwan, R. Taleei, D. Liljequist, S. Uehara, Radiation track, DNA damage and response – a review, Rep. Prog. Phys. 79 (2016) 116601. http://dx.doi.org/10.1088/0034-4885/79/11/116601.

[3] J. Lindhard, M. Scharff, Energy loss in matter by fast particles of low charge, Mat. Fys. Med. Dan. Vid. Selsk. 27 (1953) 15.

[4] R.H. Ritchie, A. Howie, Electron excitation and the optical potential in electron microscopy, Philos. Mag. 36 (1977) 463. http://dx.doi.org/10.1080/14786437708244948 (ISSN 0031-8086).

[5] C. Tung, J. Ashley, R. Ritchie, Electron inelastic mean free paths and energy losses in solids II, Surf. Sci. 81 (2) (1979) 427. http://dx.doi.org/10.1016/0039-6028(79)90110-9.

[6] J. Lindhard, K. Dan, Vidensk. Selsk. Mat.-Fys. Medd., vol. 28(8), URL http://gymarkiv.sdu.dk/MFM/kdvs/mfm.

[7] N. Mermin, Lindhard dielectric function in the relaxation-time approximation, Phys. Rev. B 1 (1970) 2362–2363. http://dx.doi.org/10.1103/physrevb.1.2362.

[8] Z.H. Levine, S.G. Louie, New model dielectric function and exchange-correlation potential for semiconductors and insulators, Phys. Rev. B 25 (1982) 6310. http://dx.doi.org/10.1103/physrevb.25.6310.

[9] M. Vos, A model dielectric function for low and very high momentum transfer, Nucl. Instrum. Method. 366 (2015) 6. http://dx.doi.org/10.1016/j.nimb.2015.09.091.

[10] H. Raether, Excitation of plasmons and interband transitions by electrons, Springer tracts in modern physics; v.88, Springer Verlag, Berlin, 1979.

[11] H. Hayashi, N. Watanabe, Y. Udagawa, C.-C. Kao, The complete optical spectrum of liquid water measured by inelastic x-ray scattering, Proc. Natl. Acad. Sci. 97 (2000) 6264. http://dx.doi.org/10.1073/pnas.110572097 (ISSN 1091-6490).

[12] H. Hayashi, N. Hiraoka, Accurate measurements of dielectric and optical functions of liquid water and liquid benzene in the VUV region (1–100 eV) using small-angle inelastic X-ray scattering, J. Phys. Chem. B 119 (2015) 5609. http://dx.doi.org/10.1021/acs.jpcb.5b01567 (URL ⟨http://dx.doi.org/10.1021/acs.jpcb.5b01567⟩).

[13] N. Watanabe, H. Hayashi, Y. Udagawa, Bethe surface of liquid water determined by inelastic X-ray scattering spectroscopy and electron correlation effects, Bull. Chem. Soc. Jpn. 70 (1997) 719. http://dx.doi.org/10.1246/bcsj.70.719.

[14] S. Manninen, T. Paakkari, V. Halonen, Experimental compton profile of water, Chem. Phys. Lett. 46 (1977) 62. http://dx.doi.org/10.1016/0009-2614(77)85163-4 (ISSN 0009-2614).

[15] D. Emfietzoglou, F.A. Cucinotta, H. Nikjoo, A complete dielectric response model for liquid water: a solution of the Bethe ridge problem, Radiat. Res. 164 (2005) 202. http://dx.doi.org/10.1667/rr3399 (ISSN 1938-5404).

[16] D. Emfietzoglou, I. Abril, R. Garcia-Molina, I. Petsalakis, H. Nikjoo, I. Kyriakou, A. Pathak, Semi-empirical dielectric descriptions of the Bethe surface of the valence bands of condensed water, Nucl. Instrum. Methods Phys. Res. Sect. B: Beam Interact. Mater. At. 266 (2008) 1154. http://dx.doi.org/10.1016/j.nimb.2007.11.057 (ISSN 0168-583X).

[17] D. Emfietzoglou, I. Kyriakou, I. Abril, R. Garcia-Molina, H. Nikjoo, Inelastic scattering of low-energy electrons in liquid water computed from optical-data models of the Bethe surface, Int. J. Radiat. Biol. 88 (2012) 22. http://dx.doi.org/10.3109/09553002.2011.588061 (ISSN 1362-3095).

[18] I. Abril, C.D. Denton, P. de Vera, I. Kyriakou, D. Emfietzoglou, R. Garcia-Molina, Effect of the Bethe surface description on the electronic excitations induced by energetic proton beams in liquid water and DNA, Nucl. Instrum. Methods Phys. Res. Sect. B: Beam Interact. Mater. At. 268 (2010) 1763–1767. http://dx.doi.org/10.1016/j.nimb.2010.02.069.

[19] F. Biggs, L. Mendelsohn, J. Mann, Hartree-Fock Compton profiles for the elements, At. Data Nucl. Data Tables 16 (1975) 201. http://dx.doi.org/10.1016/0092-640x(75)90030-3.

[20] G. Onida, L. Reining, A. Rubio, Electronic excitations: density-functional versus many-body Green's-function approaches, Rev. Mod. Phys. 74 (2002) 601. http://dx.doi.org/10.1103/revmodphys.74.601.